*Inorg. Chem.* **2005**, *44*, 4398–4406


# Boron-Induced Hydrogen Localization in the Novel Metal Hydride $LaNi_3BH_x$ ($x = 2.5$–$3.0$)

**Yaroslav E. Filinchuk* and Klaus Yvon**

*Laboratory of Crystallography, University of Geneva, 24 quai Ernest Ansermet, CH-1211 Geneva, Switzerland*

Received March 21, 2005

The crystal structure and hydrogenation properties of the intermetallic boride $LaNi_3B$ were investigated. The hydrogen-free compound has a novel structure with orthorhombic symmetry, space group *Imma*, $a = 4.9698(8)$ Å, $b = 7.1337(8)$ Å, $c = 8.3001(9)$ Å, and $V = 294.26(7)$ Å$^3$. Thermal gravimetrical analysis reveals a hydride phase that forms near ambient conditions within the compositional range $LaNi_3BH_{2.5-3.0}$. Single-crystal X-ray diffraction on both the alloy and the hydride, using the same crystal, shows an expansion in the *a*–*c* plane (by up to ∼8%) and a contraction along *b* (by ∼3%), while the symmetry changes from *Imma* to *Bmmb* (*Cmcm*) and the unit cell doubles along *a* and *b*. The cell parameters for the composition of $LaNi_3BD_{2.73(4)}$ are $a = 10.7709(7)$ Å, $b = 16.0852(10)$ Å, $c = 7.6365(5)$ Å, $V = 1323.03(15)$ Å$^3$, and space group *Cmcm*. Four nearly fully occupied interstitial hydrogen sites were located by neutron powder diffraction on deuterides and found to have tetrahedral, $La_2Ni_2$ (D1,D2), trigonal-prismatic, $La_3Ni_3$ (D3), and trigonal-bipyramidal, $La_2Ni_3$ (D4), metal environments. The structure can also be described in terms of alternating quasi two-dimensional $[NiD]^-$ slabs (Ni–D = 1.62–1.97 Å) and La–B sheets for which bond-valence sums suggest the limiting formula $La^{3+}B^0[Ni_3D_3]^{3-}$. The La–B planes do not accommodate deuterium; the B–D and D–D interactions appear to be repulsive. The shortest B–D and D–D contacts are 2.52(2) and 2.33(2) Å, respectively.

## Introduction

Only a few intermetallic borides have been studied with respect to hydrogen sorption properties. Most studies are aimed at improving the magnetic or microstructural properties of the parent ternary borides rather than investigating the crystal chemistry and sorption properties of the corresponding hydrides. Historically, the first and only boride series for which hydrogen (deuterium) atom positions have been localized by neutron diffraction is tetragonal $R_2Fe_{14}BD_x$ ($x < 3.7$, R = Y, Ce, Er).[1,2] Hydrogen was found to partially occupy tetrahedral metal interstices and had no boron atoms as nearest neighbors. Another family of intermetallic borides, $R_5Fe_2B_6$ (R = rare earth), was investigated with respect to the hydrogenation-assisted homogenization of alloys that are potentially useful for the production of hot-pressed magnets.[3,4] Hydrogenation behavior and crystal structures were reported, but the positions of the hydrogen atom were not determined. A third group of borides, with a stoichiometric composition of $RT_4B$ (R = wide range of rare earth elements, T = Fe, Co, Ni), was hydrogenated either by a solid−gas reaction[5] or by soaking in $NaBH_4$ solution.[6] While the cobalt systems displayed at least three distinct hydride phases, $RCo_4BH_x$ ($x < 4.5$), at room temperature and in the pressure range of 0−100 bar, the nickel systems absorbed only 1.5 hydrogen atoms per formula unit (f.u.) under such conditions. Finally, detailed thermodynamic, X-ray diffraction, and NMR studies on the nickel system $LaNi_4B$−$H$[5,7] were aimed at gaining further insight into the

* To whom correspondence should be addressed. Yaroslav.Filinchuk@cryst.unige.ch. Phone: +41-22-37-96372. Fax: +41-22-37-96108.

(1) Dalmas de Reotier, P.; Fruchart, D.; Pontonnier, L.; Vaillant, F.; Wolfers, P.; Yaouanc, A.; Coey, J. M. D.; Fruchart, R.; L'Heritier, P. *J. Less-Common Met.* **1987**, *129*, 133−144.
(2) Chacon, C.; Isnard, O. *J. Appl. Phys.* **2000**, *88*, 2342−2348.
(3) Yartys, V. A.; Wiesinger, G.; Harris, I. R. *J. Alloys Compd.* **1997**, *252*, 201−208.
(4) Yartys, V. A.; Denys, R. V.; Gutfleisch, O.; Bulyk, I. I.; Kuzma, Y. B.; Harris, I. R. *Int. J. Hydrogen Energy* **1999**, *24*, 189−194.
(5) Spada, F.; Oesterreicher, H. *J. Less-Common Met.* **1985**, *107*, 301−320.
(6) Kramp, S.; Febri, M.; Joubert, J. C. *J. Solid State Chem.* **1997**, *133*, 145−151.
(7) Spada, F. E.; Oesterreicher, H.; Bowman, R. C., Jr.; Guse, M. P. *Phys. Rev. B* **1984**, *30*, 4909−4924.



10.1021/ic050416j CCC: $30.25 
Published on Web 05/17/2005

mechanism of hydrogen diffusion in the well-known hydrogen storage compound $LaNi_5$. The results suggested that hydrogen occupies sites coordinated by lanthanum and nickel only, while the basal La−B planes act as barriers to hydrogen diffusion along the hexagonal axis. A mechanism and activation limiting steps for hydrogen diffusion in $LaNi_5H_x$ were suggested exploiting this "blocking" action of boron.[7] The occupancies of the suggested hydrogen sites, however, were not ascertained by independent methods.

In light of the above results, one might expect that boron has an adverse effect on the hydrogen sorption properties of intermetallic compounds because it acts as a barrier for hydrogen diffusion and favors localization of the hydrogen atoms in the metal matrix away from the boron atom sites. Structural and hydrogenation studies of borides with low boron contents are desirable for the investigation of this possibility. Here, we report on the synthesis, crystal structure, and hydrogenation properties of the ternary boride $LaNi_3B$. A phase of that composition was reported some thirty years ago by Ukrainian scientists,[8] but its crystal structure was not determined. Here, it will be shown that the boride has a novel structure and reacts with hydrogen near ambient conditions to produce a hydride with the composition $LaNi_3BH_x$ ($2.5 < x < 3.0$) in which hydrogen almost fully occupies the interstices not coordinated by boron atoms.

## Experimental Section

**Synthesis and Hydrogen Sorption Properties.** Two samples with nominal composition $LaNi_3B$, one weighing ~3 g and the other ~6 g, were prepared by arc melting lanthanum ingots (99.99%) and powder mixtures of nickel (99.9%) and boron (99.7% all from Alfa) under an argon atmosphere. The alloys were remelted three times resulting in a weight loss of ~0.1%. Laboratory X-ray powder diffraction (XRD) on the as-cast ingots revealed the presence of two well-crystallized boride phases, $La_2Ni_5B_4$ and $LaNi_4B$, with minor binary impurities. After the ingots were annealed at 800 °C in quartz tubes under 0.25 bar of argon for one month and subsequently quenched with cold water, these phases had transformed into a new boride phase, identified later as $LaNi_3B$, with more than 90% abundance for the 3 g sample and 60−80% for the 6 g sample. During the annealing process, the samples were in contact with the walls of the quartz tube. The alloy samples were activated using one hydrogen (deuterium) absorption/desorption cycle at 100 bar/$3 \times 10^{-2}$ mbar of pressure for 1 day at 20 °C, and then they were charged with hydrogen (4N, Carbagas) or deuterium (99.4%, AGA) in an autoclave at room temperature and 100 bar of pressure for 2 days. The reaction product was a fine black powder that could be handled in air without detectable oxide formation during the subsequent diffraction experiments. A thermogravimetrical analysis (TGA) of hydrogen absorption was performed at room temperature on a Hiden Analytical Intelligent Gravimetric Analyzer with 50 mg of a finely ground fraction of the annealed alloy (3 g sample), containing 92% of the main phase. The applied hydrogen pressure varied from $10^{-2}$ to 7 bar at room temperature and 100 °C. The absorption kinetics on the first cycle of hydrogenation were fairly slow as can be seen from the pressure−composition isotherm recorded during the first 48 h (Figure 1).

**Single-Crystal X-ray Diffraction.** A single crystal was extracted from the 3 g $LaNi_3B$ alloy used for the TGA and desorption

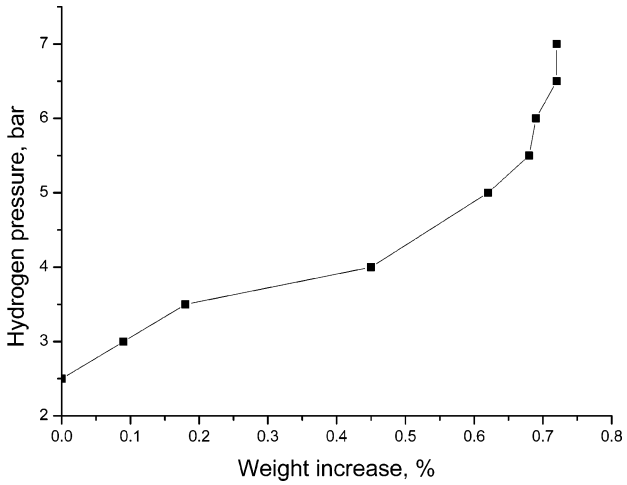


**Figure 1.** Pressure−composition isotherm of $LaNi_3BH_x$ at 20 °C; the maximum hydrogen content was 2.4 H/f.u. on the first cycle of hydrogen absorption.

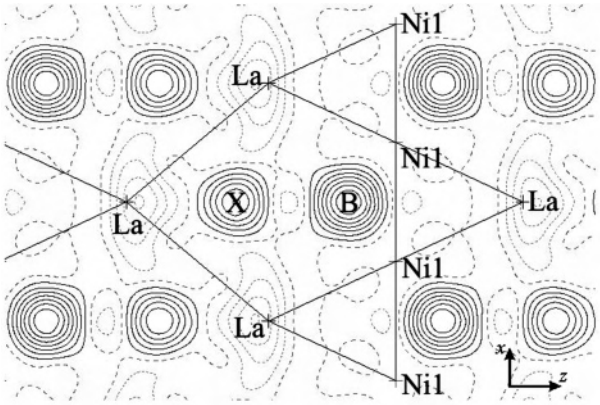


**Figure 2.** $x1/4z$ section of the difference Fourier map for $LaNi_3B$ calculated from the single-crystal XRD data and the coordinates of La and Ni atoms.

experiments, mounted on a glass fiber, and measured on a Stoe IPDS II diffractometer equipped with an image plate detector and Mo X-ray tube; 110 $\omega$ oscillation images with a 1° increment were collected at 20(1) °C with 5 and 1 min exposure times for each image (crystal to detector distance 40 mm). The data were corrected for the Lorentz factor and polarization effects, and they were also corrected numerically for absorption (8 faces for a trigonal prismatic-like crystal, $V = 9.1 \times 10^{-5}$ mm$^3$, $\mu = 32.8$ mm$^{-1}$, $T_{min,max} = 0.249, 0.411$). Cell parameters were obtained by a least-squares refinement of 5688 reflection angles in the range $9.6° < 2\theta < 76.7°$. No variation of the average intensity was observed during the measurement. A small randomly twinned domain (less that 2% of the total scattering power) was identified and sorted out during the intensity integration procedure. No warnings for twinning or superstructure were observed thereafter. The systematic extinctions indicated space group *Imma*. The metal atom substructure (1 La and 2 Ni sites) was solved by direct methods,[9] and the subsequent difference Fourier synthesis revealed two electron density peaks (labeled B and X in Figure 2). The least-squares refinement of peaks B and X suggested a scattering power corresponding to 100% and 79(4)%, respectively, of boron. However, as will be shown below the origin of the X peak is unlikely to be boron. A full least-squares refinement on $F^2$ up to 65.6° for $2\theta$ was performed on positional

(8) Kuz′ma, Yu. B.; Bilonizhko, N. S.; Nimkovich, E. M. *Dopov. Akad. Nauk Ukr. RSR, Ser. A* **1973**, *35*, 939−941.

(9) Sheldrick, G. M. *SHELXS97 and SHELXL97. Programs for the solution and refinement of crystal structures*; University of Göttingen: Göttingen, Germany, 1997.

**Table 1.** Single-Crystal Data and Details of Data Collection and Structure Refinement for $LaNi_3B$ and $LaNi_3BH_{\sim 2.7}$

| | | |
|---|---|---|
| empirical formula | $LaNi_3B$ | $LaNi_3BH_{\sim 2.7}$ |
| fw | 325.85 (X not included) | 325.85 (H atoms not included) |
| cryst syst, space group | orthorhombic, *Imma* | orthorhombic, *Cmcm* |
| $a$ (Å) | 4.9698(8) | 10.769(2) |
| $b$ (Å) | 7.1337(8) | 16.164(3) |
| $c$ (Å) | 8.3001(9) | 7.6414(12) |
| $V$ (Å$^3$) | 294.26(7) | 1330.2(4) |
| $Z$, $D_c$ (g·cm$^{-3}$) | 4, 7.355 | 16, 6.508 |
| $F$(000) | 584 | 2336 |
| index ranges | $-7 \le h \le 6$ | $-12 \le h \le 12$ |
| | $-10 \le k \le 9$ | $-17 \le k \le 19$ |
| | $-11 \le l \le 12$ | $-9 \le l \le 8$ |
| $2\theta_{max}$ (deg)/completeness (%) | 65.6/95.4 | 50/96.2 |
| $R_{int}/R_\sigma$ | 0.0304/0.0127 | 0.1154/0.0654 |
| reflns collected/unique | 2112/322 | 3787/667 |
| data/restraints/parameters | 322/0/19 | 667/0/51 |
| final $R$ indices [$I > 2\sigma(I)$] | $R_1 = 0.0247$ | $R_1 = 0.0684$ |
| | $R_2 = 0.0543$ | $R_2 = 0.1600$ |
| $R$ indices (all data) | $R_1 = 0.0250$ | $R_1 = 0.0868$ |
| | $R_2 = 0.0545$ | $R_2 = 0.1673$ |
| GOF on $F^2$ | 1.153 | 1.148 |
| extinction coefficient | 0.0083(7) | − |
| $(\Delta/\sigma)_{max}$ | 0.000 | 0.000 |
| largest diff. peak and hole (e/Å$^{-3}$) | 3.2(3) and −2.1(3) | 2.5(4) and −1.7(4) |

and thermal parameters for all of the atoms (anisotropic for La and Ni) using SHELXL-97.[9] Reduced cell calculations and noncrystallographic symmetry checks (PLATON2003[10]) did not indicate higher lattice symmetry or missing symmetry elements. Trial refinements in the noncentrosymmetric space groups, *I2ma*, *Im2a*, and *Imm*2, yielded inferior results.

After data collection, the alloy crystal was removed from the diffractometer and, while still on the glass fiber, placed into an autoclave, vacuum pumped, and hydrogenated at 50 °C and 30 bar for 2 days. Microscopic examination showed that the crystal had cracked upon hydrogenation, but a fraction of ∼40% was still present on the glass fiber; 180 $\omega$ oscillation images with a 1° increment were collected at 20(1) °C with a 10 min exposure time per image (crystal to detector distance 120 mm). The data were numerically corrected for absorption (7 faces for a wedge-like crystal, $V = 3.3 \times 10^{-5}$ mm$^3$, $\mu = 29.0$ mm$^{-1}$, $T_{min,max} = 0.326$, 0.641). While their symmetry remained orthorhombic, they showed a new C-centered supercell four times bigger than that of the alloy structure and a volume increase of about 13% (see Table 1). A comparison with the neutron powder diffraction data (see below) collected on a sample with a similar volume increase suggested that the hydrogen content was ∼2.7 H/f.u. During data collection (35 h), the cell volume decreased smoothly by ∼0.6% suggesting some hydrogen desorption; this was accounted for during intensity integration. Two randomly twinned domains of comparable scattering power were identified. Only about 5% of the reflections were overlapped and therefore neglected during intensity integration. The data set for one of the domains was used afterward. Cell parameters were obtained by a least-squares refinement of 3403 reflection angles in the range $4.6° < 2\theta < 54.0°$. The systematic extinctions indicated space group *Cmcm*. The metal atom substructure (3 La and 4 Ni sites) was solved by direct methods. Three boron atoms were clearly localized from a difference Fourier map as 5.6−5.8 e/Å$^3$ peaks. The next highest residual electron density peak of 2.3 e/Å$^3$ was found ∼0.9 Å from the La atom and is presumably the result of series termination effects, anharmonicity effects, or both. Interestingly, no significant electron density was found to occur on site X unlike that found in the alloy. Structure refinement and validation were performed in the same manner as for the alloy.

**Table 2.** Atomic Coordinates and Thermal Parameters in $LaNi_3B$ and $LaNi_3BH_{\sim 2.7}$ from the Single-Crystal Data

$LaNi_3B$ (*Imma*)

| atom | Wyckoff site | $x$ | $y$ | $z$ | $U_{eq/iso}$ (Å$^2$) |
|---|---|---|---|---|---|
| La | 4*e* | 0 | 1/4 | 0.56990(6) | 0.01244(18) |
| Ni1 | 8*g* | 1/4 | 0.07336(10) | 1/4 | 0.0082(2) |
| Ni2 | 4*a* | 0 | 0 | 0 | 0.0133(3) |
| B | 4*e* | 0 | 1/4 | 0.1292(12) | 0.0130(15) |
| X[a] | 4*e* | 0 | 1/4 | 0.8554(15) | 0.0130(15) |

$LaNi_3BH_{2.7}$ (*Cmcm*)

| atom | Wyckoff site | $x$ | $y$ | $z$ | $U_{eq/iso}$ (Å$^2$) |
|---|---|---|---|---|---|
| La1 | 8*g* | 0.27772(17) | 0.27594(12) | 1/4 | 0.0307(6) |
| La2 | 4*c* | 0 | 0.45517(18) | 1/4 | 0.0333(7) |
| La3 | 4*c* | 0 | 0.97140(15) | 1/4 | 0.0275(7) |
| Ni1 | 16*h* | 0.1185(2) | 0.13021(16) | 0.0847(4) | 0.0264(7) |
| Ni2 | 16*h* | 0.3682(2) | 0.11693(17) | 0.0888(4) | 0.0305(7) |
| Ni3 | 8*f* | 0 | 0.2641(2) | 0.0258(6) | 0.0293(10) |
| Ni4 | 8*e* | 0.2338(3) | 0 | 0 | 0.0306(10) |
| B1 | 8*g* | 0.237(3) | 0.073(2) | 1/4 | 0.027(7) |
| B2 | 4*c* | 0 | 0.192(3) | 1/4 | 0.033(11) |
| B3 | 4*c* | 0 | 0.661(4) | 1/4 | 0.037(12) |

[a] A peak of the residual electron density was modeled by a position X, 79(4)% occupied by boron atoms.

Crystal data and the details of data collection[11] and structure refinement[9] are given in Table 1. The relatively high $R$ factors are a consequence of the small size of the hydride crystal and are close to the ratio $R_{int}/R_\sigma$ which describes the intrinsic quality of the data. The atomic positions for $LaNi_3B$ and $LaNi_3BH_{2.7}$, as standardized with the STRUCTURE TIDY program,[12] are listed in Table 2, and interatomic distances are given in Table 3.

**Analysis of Electron Density by the Maximum-Entropy Method (MEM).** In light of the importance of residual electron density features in the crystal investigated, we performed an additional MEM analysis. This model-free image reconstruction method[13] is capable of providing reliable results as shown, for example, during the study of partially occupied oxygen sites in Hg-based high-$T_C$ superconductors[14] and the identification of tiny disorders in intermetallic compounds.[15] The electron density

(10) Spek, A. L. *PLATON. A Multipurpose Crystallographic Tool*; University of Utrecht: Utrecht, The Netherlands, 2003.

(11) *X-RED and X-Area Software*; Stoe & Cie: Darmstadt, Germany, 2003.
(12) Gelato, L. M.; Parthé, E. *J. Appl. Crystallogr.* **1987**, *20*, 139−143.
(13) Gilmore, C. J. *Acta Crystallogr. A* **1996**, 561−589.
(14) Papoular, R. J.; Collin, G.; Colson, D.; Viallet, V. *AIP Conf. Proc.* **2002**, *617*, 204−226.

**Table 3.** Interatomic Distances (Å) in $LaNi_3B$ and $LaNi_3BH_{\sim 2.7}$ from Single-Crystal XRD[a]

| $LaNi_3B$ | | $LaNi_3BH_{\sim 2.7}$ | |
|---|---|---|---|
| La-4Ni1 | 3.0165(7) | La1-8Ni | 3.012(3)-3.254(3) |
| La-4Ni2 | 3.1132(4) | La1-2B | 3.03(4)-3.28(2) |
| La-4Ni1 | 3.1909(7) | La2-8Ni | 3.174(3)-3.220(4) |
| La-2B | 2.984(6) | La3-12Ni | 3.133(3)-3.297(3) |
| | | La3-2B1 | 3.04(3) |
| Ni1-2La | 3.0165(7) | Ni1-5La | 3.133(3)-3.297(3) |
| Ni1-2La | 3.1909(7) | Ni1-5Ni | 2.526(4)-2.698(3) |
| Ni1-2Ni2 | 2.4745(3) | Ni1-2B | 2.02(3)-2.06(2) |
| Ni1-2Ni1 | 2.4849(4) | Ni2-3La | 3.012(3)-3.220(4) |
| Ni1-Ni1 | 2.5202(15) | Ni2-5Ni | 2.464(4)-2.839(3) |
| Ni1-2B | 2.034(5) | Ni2-2B | 2.00(3)-2.01(2) |
| Ni2-4La | 3.1132(4) | Ni3-2La1 | 3.254(3) |
| Ni2-4Ni1 | 2.4745(3) | Ni3-4Ni | 2.546(4)-2.552(4) |
| Ni2-2B | 2.081(5) | Ni3-2B | 2.07(3)-2.43(3) |
| | | Ni4-3La3 | 3.194(3) |
| | | Ni4-4Ni | 2.475(3)-2.528(3) |
| | | Ni4-2B | 2.246(17) |
| B-2La | 2.984(6) | B1-La3 | 3.04(3) |
| B-4Ni1 | 2.034(5) | B1-2Ni2 | 2.00(3) |
| B-2Ni2 | 2.081(5) | B1-2Ni1 | 2.02(3) |
| | | B1-2Ni4 | 2.246(17) |
| | | B2-4Ni1 | 2.06(2) |
| | | B2-2Ni3 | 2.07(3) |
| | | B3-2La1 | 3.03(4) |
| | | B3-4Ni2 | 2.01(2) |
| | | B3-2Ni3 | 2.43(3) |
| X-2Ni2 | 2.150(7) | | |
| X-La | 2.370(13) | | |
| X-2La | 2.561(3) | | |
| X-4Ni2 | 2.762(4) | | |

[a] Coordination spheres are limited to 3.3 Å for La and Ni atoms and to 3.1 Å for B atoms.

distribution in the $LaNi_3B$ crystal was calculated by the BayMEM program[16] using the experimental structure amplitudes, $F_{obs}$, from the single-crystal experiment corrected for anomalous scattering. The phases of the reflections were taken from the computed structure factors of two models, one excluding and the other including the X peak with a scattering power corresponding to a boron atom. The standard uncertainties, $\sigma(F_{obs})$, used to define the end of the MEM iterations were derived from the experimentally observed variance of symmetry equivalent reflections. The expected number of electrons per unit cell was fixed at 584, corresponding to four $LaNi_3B$ f.u./cell. The MEM calculations used the electron densities from the two models as prior electron densities. A perfectly clear map (not shown here) without spurious peaks was obtained; it confirms that the previously identified electron density maximum at the X position corresponds to the scattering power of 45−68% of boron. A summary of the MEM results is given in Table 4. Although a noise-free MEM map with a clear X peak is a proof that electron density is localized in this position, the integrated electronic populations should be interpreted only qualitatively. The true electron populations are presumably within the limits of the two models whose spread represents the experimental uncertainty.

**Table 4.** Integrated Properties of Bader Topological Atoms[35] in the MEM Density of $LaNi_3B$ with and without Electron Density Peak X Included in the Prior Electron Density

| atom | atomic volume (Å$^3$) | electronic population ($e^-$) |
|---|---|---|
| La | 21.76/22.18 | 54.50/55.23 |
| Ni1 | 13.90/13.34 | 28.27/27.63 |
| Ni2 | 12.91/11.42 | 27.83/27.28 |
| B | 7.55/7.56 | 5.07/4.95 |
| X | 4.21/6.18 | 2.24/3.38 |

**Synchrotron Powder Diffraction.** Both the alloy and hydride structures were studied by high-resolution synchrotron powder diffraction to confirm the absence of possibly overlooked superstructure peaks. The alloy sample used for the single-crystal and TGA experiments and the hydride sample obtained during the TGA experiment were put into thin-walled glass capillaries with a diameter of 0.3 mm and measured with Debye−Scherrer geometry on the Swiss−Norwegian beam line (BM1) at ESRF (Grenoble, France). Six Si(111) analyzers were used to record the diffraction pattern at $\lambda = 0.500$ Å in the $2\theta$ range 3.0−45.5° ($d_{min} = 0.68$ Å) with a step size of 0.004° for the alloy and in the $2\theta$ range 3.0−38.3° ($d_{min} = 0.79$ Å) with a step size of 0.005° for the hydride. Each diffraction pattern was recorded in approximately 4 h. Structure refinement was carried out with the FULLPROF SUITE[17] starting with the atomic coordinates derived from the single-crystal XRD experiment. An absorption correction was applied by assuming $\mu r = 1$.

For the alloy sample, the following 38 parameters were refined:[18] 3 scale factors, 9 cell parameters for the three identified phases (91.5(3)% $LaNi_3B$, 4.65(8)% $La_2Ni_5B_4$, and 3.83(6)% $LaNi_4B$), and 26 parameters for the phase of interest ($LaNi_3B$), of which there are 6 profile and 3 microstrain parameters (accounting for anisotropic line broadening), 4 positional and 12 thermal parameters (anisotropic for La and Ni atoms), and 1 occupancy parameter for the X position. The latter was modeled by an atom scattering power of 68(2)% of boron. The diffraction pattern is presented in Figure 3. Atom coordinates (listed in the Supporting Information) are equal within eight standard uncertainties to those found from the single-crystal XRD experiment; the difference in atomic positions is 0.007 Å for La, 0.002 Å for Ni, and 0.02 Å for B and X. It is highly

(15) Cargnoni, F.; Nishibori, E.; Rabiller, P.; Bertini, L.; Snyder, G. J.; Christensen, M.; Gatti, C.; Iversen, B. B. *Chem.—Eur. J.* **2004**, *10*, 3861−3870.
(16) van Smaalen, S.; Palatinus, L.; Schneider, M. *Acta Crystallogr. A* **2003**, *59*, 459−469.
(17) Rodriguez-Carvajal, J. *FULLPROF SUITE*; LLB Sacley & LCSIM: Rennes, France, 2003.
(18) Phase 1: $LaNi_3B$, 91.5(3)%, *Imma*, $a = 4.97675(3)$ Å, $b = 7.14917(4)$ Å, $c = 8.30753(6)$ Å, $V = 295.579(3)$ Å$^3$, $R_B = 0.0281$, $R_F = 0.0311$, $\chi^2 = 2.45$, $R_p = 0.0632$, $R_{wp} = 0.0808$, number of independent reflections = 944, number of effective reflections (accounting resolution) = 235. Phase 2: $La_2Ni_5B_4$, 4.65(8)%. Phase 3: $LaNi_4B$, 3.83(6)%.

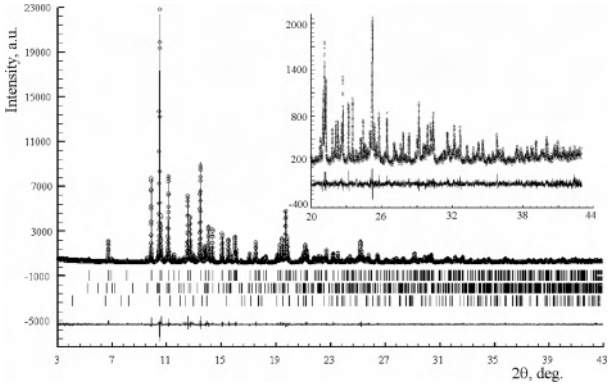


**Figure 3.** Observed (points), calculated (line), and difference (bottom line) synchrotron diffraction patterns for the $LaNi_3B$ alloy; $\lambda = 0.50014(1)$ Å. Vertical bars indicate the Bragg positions of the contributing phases.[18]

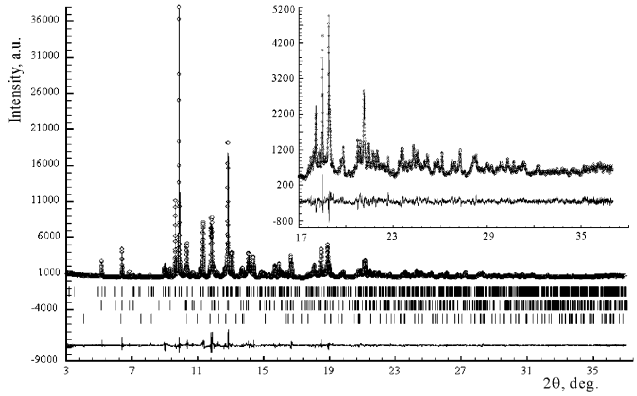


**Figure 4.** Observed (points), calculated (line), and difference (bottom line) synchrotron diffraction patterns for the $LaNi_3BH_{\sim 2.5}$ hydride; $\lambda = 0.50014(1)$ Å. Vertical bars indicate the Bragg positions of the contributing phases.[19]

satisfactory that the shape and orientation of the anisotropic thermal displacement ellipsoids remained nearly unchanged. No superstructure peaks were detected in the difference pattern.

For the hydride sample the following 51 parameters were refined:[19] 3 scale factors, 9 cell parameters for the three identified phases (90.0(5)% $LaNi_3BH_{\sim 2.5}$, 6.4(3)% $La_2Ni_5B_4H_{\sim 2}$ and 3.6(2)% $LaNi_4BH_{\sim 1.5}$), 9 structural and profile parameters for the secondary phases ($La_2Ni_5B_4H_{\sim 2}$ and $LaNi_4BH_{\sim 1.5}$), and 30 for the phase of interest ($LaNi_3BH_{\sim 2.5}$), of which there are 8 profile and 3 microstrain parameters (accounting for anisotropic line broadening) and 17 positional and 2 overall isotropic thermal parameters (for the La and Ni and B atoms, respectively). The diffraction pattern is presented in Figure 4. The superstructure peaks are consistent with the cell data and space group derived from the single-crystal XRD experiment. Atom coordinates (listed in the Supporting Information) for La and Ni are equal within a few standard uncertainties to those found from the single-crystal XRD experiment. In contrast to that found in the alloy, no significant electron density appeared on the X site.

**Neutron Powder Diffraction (NPD).** The alloy samples were deuterated at 25 °C under 100 bar of $D_2$. One sample (~2.5 g) was prepared 4 months before the NPD experiment and contained ~90% of the main phase, and the other (~6 g) was prepared 1 day before the experiment and contained ~80% of the main phase. To reduce the severe absorption of the neutron flux by the natural boron isotope mixture, we used double-walled vanadium cylinders (30−40 mm in length and 8 mm external/6 mm internal diameter for the first sample and 9 mm external/5 mm internal diameter for the second sample, both sealed by an indium wire). Diffraction patterns were collected on the high-resolution powder diffractometer HRPT at SINQ (PSI, Villigen, Switzerland) in high-intensity mode ($\lambda$ = 1.494 Å, $2\theta$ range 4−164°, $d_{min}$ = 0.75 Å, step size 0.1°, data collection time ~13 h for each sample). The precise values of wavelengths were determined from the measurements of a standard silicon sample. Structure refinement was carried out with the FULLPROF SUITE program package[17] starting with metal atom parameters derived from the single-crystal XRD experiment. Four deuterium atoms were located on difference nuclear density Fourier maps (D1−D4). There was no indication of a significant scattering density at the X site as was found in the single-crystal experiment on the alloy.

The following 57 parameters were refined for each sample:[20,21] 3 scale factors, 1 zero shift, 9 cell parameters for the three identified phases ($LaNi_3BD_x$, $La_2Ni_5B_4D_x$, $LaNi_4BD_x$), 2 structural parameters for secondary phases ($La_2Ni_5B_4D_x$, $LaNi_4BD_x$) and the phase of interest ($LaNi_3BD_x$), 5 profile and 3 microstrain parameters to model anisotropic line broadening (orthorhombic strain model no. 10),[17] 26 positional parameters, 4 overall isotropic thermal parameters (La, Ni, B, D), and 4 occupancy factors for the D sites. The absorption correction was applied using experimentally determined attenuation coefficients ($\mu_r$ = 0.40 and 0.83 for the first and second samples, respectively). The refined deuterium occupancies suggest slightly different compositions, $LaNi_3BD_{2.51(5)}$ and $LaNi_3BD_{2.73(4)}$, for the first and second samples, respectively. This difference correlates with the unit cell volumes and is consistent with the fact that the second sample was prepared closer to the NPD experiment than the first one and thus had less time to desorb. Atom coordinates for both samples are listed in Table 5, and selected interatomic distances are given in Table 6. The diffraction pattern for the first, 90% pure, sample is presented in Figure 5.

## Results and Discussion

**Structure of $LaNi_3B$.** In contrast to the known borides with the composition $RT_3B$ (R = rare earth element, T = transition metal) that crystallize with cubic perovskite-type structures, such as $RPd_3B$,[22] or tetragonal deformation derivatives, such as $CePt_3B$,[23] $LaNi_3B$ crystallizes with an orthorhombic structure that can be considered a novel defect variant of the hexagonal $CeCo_3B_2$-type structure (for a review on deformation variants of that structure type see ref 24).

(19) Phase 1: $LaNi_3BH_{\sim 2.5}$, 90.0(5)%, *Cmcm*, $a$ = 10.74979(16) Å, $b$ = 16.1381(3) Å, $c$ = 7.63906(13) Å, $V$ = 1325.23(4) Å$^3$, $R_B$ = 0.0509, $R_F$ = 0.0364, $\chi^2$ = 6.91, $R_p$ = 0.0687, $R_{wp}$ = 0.0939, number of independent reflections = 2061, number of effective reflections (accounting resolution) = 254. Phase 2: $La_2Ni_5B_4H_{\sim 2}$, 6.4(3)%. Phase 3: $LaNi_4BH_{\sim 1.5}$, 3.6(2)%.

(20) Phase 1: $LaNi_3BD_{2.51(5)}$, 90(1)%, *Cmcm*, $a$ = 10.7155(10) Å, $b$ = 16.1598(14) Å, $c$ = 7.6134(6) Å, $V$ = 1318.33(19) Å$^3$, $R_B$ = 0.0442, $R_F$ = 0.0262, $\chi^2$ = 3.61, $R_p$ = 0.0152, $R_{wp}$ = 0.0203, number of independent reflections = 1405, number of effective reflections (accounting resolution) = 187. Phase 2: $La_2Ni_5B_4D_{\sim 2}$, 6.2(4)%. Phase 3: $LaNi_4BD_{\sim 1.5}$, 3.8(3)%.

(21) Phase 1: $LaNi_3BD_{2.73(4)}$, 83(1)%, *Cmcm*, $a$ = 10.7709(7) Å, $b$ = 16.0852(10) Å, $c$ = 7.6365(5) Å, $V$ = 1323.03(15) Å$^3$, $R_B$ = 0.0468, $R_F$ = 0.0291, $\chi^2$ = 4.90, $R_p$ = 0.0195, $R_{wp}$ = 0.0251, number of independent reflections = 1452, number of effective reflections (accounting resolution) = 220. Phase 2: $La_2Ni_5B_4D_{\sim 2}$, 8.0(4)%. Phase 3: $LaNi_4BD_{\sim 1.5}$, 8.6(3)%.

(22) Malik, S. K.; Dhar, S. K.; Vijayaraghavan, R. *Bull. Mater. Sci.* **1984**, *6*, 263−272.

(23) Sologub, O. L.; Hester, J. R.; Salamakha, P. S.; Leroy, E.; Godart, C. *J. Alloys Compd.* **2002**, *337*, 10−17.

(24) Cenzual, K.; Chabot, B.; Parthé, E. *Acta Crystallogr. C* **1988**, *44*, 221−226.

**Table 5.** Crystal Structure Data of $LaNi_3BD_{2.51(5)}$[20] (upper lines in italic) and $LaNi_3BD_{2.73(4)}$[21] (lower lines in bold) Refined from Neutron Powder Diffraction Data[a]

| atom | Wyckoff site | *x* | *y* | *z* | $U_{iso}$ (Å$^2$) | occupancy |
|---|---|---|---|---|---|---|
| La1 | 8*g* | *0.2703(10)* | *0.2712(7)* | 1/4 | *0.0105(13)* | |
| | | **0.2764(8)** | **0.2755(6)** | | **0.0169(11)** | |
| La2 | 4*c* | 0 | *0.4504(10)* | 1/4 | | |
| | | | **0.4543(8)** | | | |
| La3 | 4*c* | 0 | *0.9693(11)* | 1/4 | | |
| | | | **0.9744(8)** | | | |
| Ni1 | 16*h* | *0.1188(11)* | *0.1282(5)* | *0.0811(8)* | *0.0084(4)* | |
| | | **0.1193(7)** | **0.1302(4)** | **0.0816(7)** | **0.0131(3)** | |
| Ni2 | 16*h* | *0.3719(10)* | *0.1136(4)* | *0.0925(8)* | | |
| | | **0.3675(6)** | **0.1139(3)** | **0.0900(7)** | | |
| Ni3 | 8*f* | 0 | *0.2607(6)* | *0.0216(11)* | | |
| | | | **0.2647(5)** | **0.0306(8)** | | |
| Ni4 | 8*e* | *0.2317(9)* | 0 | 0 | | |
| | | **0.2344(7)** | | | | |
| B1 | 8*g* | *0.2393(19)* | *0.0703(14)* | 1/4 | *0.0131(18)* | |
| | | **0.2381(14)** | **0.0682(8)** | | **0.0147(14)** | |
| B2 | 4*c* | 0 | *0.193(2)* | 1/4 | | |
| | | | **0.1946(14)** | | | |
| B3 | 4*c* | 0 | *0.6696(19)* | 1/4 | | |
| | | | **0.6599(12)** | | | |
| D1 | 16*h* | *0.1043(14)* | *0.3287(8)* | *0.077(2)* | *0.040(3)* | *0.98(3)* |
| | | **0.1090(10)** | **0.3334(6)** | **0.0874(18)** | **0.0324(14)** | **0.92(3)** |
| D2 | 16*h* | *0.3149(18)* | *0.4074(11)* | *0.103(2)* | | *0.83(3)* |
| | | **0.3216(12)** | **0.4135(7)** | **0.0977(17)** | | **0.89(3)** |
| D3 | 8*f* | 0 | *0.1793(18)* | *0.576(3)* | | *0.71(4)* |
| | | | **0.1722(10)** | **0.5764(20)** | | **0.85(3)** |
| D4 | 8*e* | *0.387(2)* | 0 | 0 | | *0.69(4)* |
| | | **0.3847(14)** | | | | **0.99(3)** |

[a] Overall isotropic temperature factors were used for each atom type. All sites, except the deuterium sites, are fully occupied.

**Table 6.** Selected Interatomic Distances (Å) and Angles (deg) in $LaNi_3BD_{2.73(4)}$ from NPD[a]

| | | | | | | | |
|---|---|---|---|---|---|---|---|
| | | | | Ni atoms | | | |
| Ni1−Ni1 | 2.570(10) | Ni2−Ni1 | 2.687(9) | Ni3−2Ni1 | 2.546(10) | Ni4−2Ni1 | 2.512(8) |
| Ni1−Ni1 | 2.572(7) | Ni2−Ni2 | 2.854(9) | Ni3−2Ni2 | 2.588(8) | Ni4−2Ni2 | 2.426(7) |
| Ni1−Ni2 | 2.687(9) | Ni2−Ni2 | 2.444(7) | | | | |
| Ni1−Ni3 | 2.546(10) | Ni2−Ni3 | 2.588(8) | | | | |
| Ni1−Ni4 | 2.512(8) | Ni2−Ni4 | 2.426(7) | | | | |
| Ni1−B1 | 2.070(13) | Ni2−B1 | 1.994(13) | Ni3−B2 | 2.020(14) | Ni4−2B1 | 2.202(7) |
| Ni1−B2 | 2.092(13) | Ni2−B3 | 2.019(9) | Ni3−B3 | 2.463(12) | | |
| Ni1−D2 | 1.665(14) | Ni2−D1 | 1.618(14) | Ni3−2D1 | 1.670(12) | Ni4−2D2 | 1.690(12) |
| Ni1−D3 | 1.888(13) | Ni2−D4 | 1.966(5) | Ni3−D3 | 1.698(18) | Ni4−D4 | 1.619(17) |
| D2−Ni1−D3 | 83.4(9) | D1−Ni2−D4 | 100.4(7) | D1−Ni3−D1 | 89.3(9) | D2−Ni4−D2 | 138.1(12) |
| | | | | D1−Ni3−D3 | 134.8(14) | D2−Ni4−D4 | 110.9(12) |
| | | | | B atoms | | | |
| B1−2Ni1 | 2.070(13) | B2−4Ni1 | 2.092(13) | B3−4Ni2 | 2.019(9) | | |
| B1−2Ni2 | 1.994(13) | B2−2Ni3 | 2.020(14) | B3−2Ni3 | 2.463(12) | | |
| B1−2Ni4 | 2.202(7) | | | | | | |
| | | | | D atoms | | | |
| D1−La1 | 2.379(14) | D2−La1 | 2.553(15) | D3−2La1 | 2.875(12) | D4−2La2 | 2.393(9) |
| D1−La2 | 2.589(15) | D2−La3 | 2.450(14) | D3−La3 | 2.70(2) | | |
| D1−Ni2 | 1.618(14) | D2−Ni1 | 1.665(14) | D3−2Ni1 | 1.888(13) | D4−2Ni2 | 1.966(5) |
| D1−Ni3 | 1.670(12) | D2−Ni4 | 1.690(12) | D3−Ni3 | 1.698(18) | D4−Ni4 | 1.619(17) |
| Ni2−D1−Ni3 | 103.8(8) | Ni1−D2−Ni4 | 96.9(8) | Ni1−D3−Ni1 | 85.8(7) | Ni2−D4−Ni2 | 169.2(5) |
| | | | | Ni1−D3−Ni3 | 90.4(9) | Ni2−D4−Ni4 | 84.6(7) |

[a] Coordination spheres are limited to 3.0 Å for Ni atoms and to first nearest neighbors for B and D atoms.

Other known boron deficient derivatives of the $CeCo_3B_2$-type structure are hexagonal $LiPt_3B$ and $NaPt_3B_{1+x}$ and orthorhombic $Na_3Pt_9B_5$.[25] As shown in Figures 6 and 7, the boron atoms in $LaNi_3B$ are coordinated by a strongly deformed trigonal prism of Ni atoms at bond distances of B−Ni1 = 2.03 Å and B−Ni2 = 2.08 Å with two side faces capped by La atoms at 2.98 Å (Table 3). This type of coordination is the most common among intermetallic boride structures.[26,27] Lanthanum is coordinated by a distorted hexagonal prism of nickel atoms; two of the $Ni_4$ faces are capped by boron atoms. The La atoms are situated in

(25) Mirgel, R.; Jung, W. *J. Less-Common Met.* **1988**, *144*, 87−99.

(26) Rogl, P. In *Modern Perspectives in Inorganic Crystal Chemistry*; Parthé, E., Ed.; NATO ASI Series; Kluwer: Norwell, MA, 1992; pp 267−278.

(27) Kuz′ma, Yu. B. *Crystal Chemistry of Borides* (in Russian); Vyshcha Shkola Press: Lvov, Ukraine, 1983.

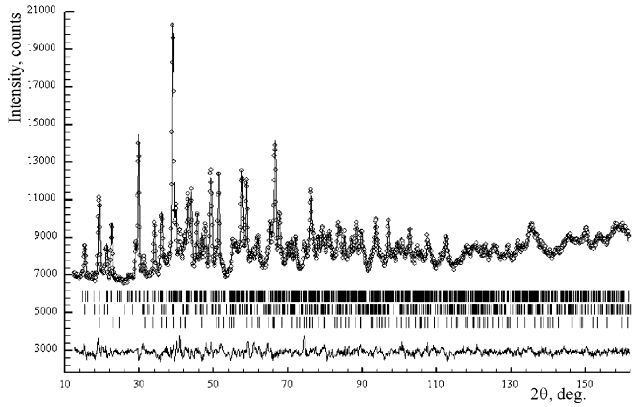


**Figure 5.** Observed (points), calculated (line), and difference (bottom line) NPD patterns for the $LaNi_3BD_{2.51(5)}$; $\lambda = 1.493814(19)$ Å. Vertical bars indicate the Bragg positions of the contributing phases.[20]

distorted hexagonal arrays of nickel prisms of which only half are filled by boron. Compared to the hexagonal $CeCo_3B_2$-type structure, in which all of the transition metal prisms are filled by boron, the La atoms in $LaNi_3B$ move away from the center of the nickel prism arrays toward the empty Ni prisms; this alters those filled by boron atoms along *b* (see Figure 6a). This presumably causes the orthorhombic distortion of the structure. Nickel is either 11-fold (Ni1, $[La_4Ni_5B_2]$) or 10-fold (Ni2, $[La_4Ni_4B_2]$) coordinated. Interestingly, one of the sites (Ni2) shows a pronounced anisotropy of its thermal displacements (Figure 7a) that preludes a site-symmetry reduction in the hydride structure (see below). As can be seen in Table 4, the MEM results are consistent with nearly neutral nickel and boron and cationic lanthanum.

The X electron density peak is situated within the empty Ni prisms, but it is unlikely to represent a (partially occupied) boron atom position for the following reasons. First, its coordination polyhedron (distorted trigonal bipyramid with three basal La and two apical Ni atoms, Table 3) does not correspond to that usually observed for boron in intermetallic boride structures.[27] Second, the La−X distances (2.37 and 2.56 Å) are much shorter that the La−B distances commonly found in intermetallic borides (>3.0 Å) and even shorter than those in the lanthanum bromide carbide boride, $La_9Br_5(CBC)_3$ (La−B = 2.64(2) Å).[28] Third, if the X site were partially occupied by boron, the resulting overall composition ($LaNi_3B_{1.7}$) would by far exceed the uncertainty of the experimental composition ($LaNi_3B$) which was controlled during the alloy preparation at a level of ∼1 at. % B. Finally, no scattering intensity was detected on the X site in the hydride (deuteride) structure as determined by single-crystal XRD (on the same crystal) and synchrotron and neutron powder diffraction which leads to the stoichiometric composition $LaNi_3B$ for the metallic matrix. A more likely origin for the X peak in the alloy is contamination by oxygen during the long-term annealing in the quartz ampule at 800 °C. In fact, a bond-valence sum calculation[29] for an oxygen atom at this site yields a value of 1.81, in good agreement with the expected value (2). The fact that this peak disappears in the hydride (deuteride) could be related to a reduction of oxygen by hydrogen. Another possible interpretation of the X peak as a nonnuclear electron density maximum resulting from La−La interactions, especially in view of the recent discovery of Ta−Ta three-center bonds in $ScTaN_2$,[30] should lead to an electron density with a much smaller magnitude.

**Hydrogenation Properties.** $LaNi_3B$ is capable of absorbing hydrogen near ambient conditions. As can be seen in Figure 1, the equilibrium pressure of the hydride phase $LaNi_3BH_x$ measured during the first cycle of hydrogenation (48 h) is not well characterized and is estimated to be around 4 bar at 25 °C. The hydrogen content was estimated after the first cycle of hydrogenation to be 2.4 H/f.u. The more or less continuous increase in the decomposition pressure at higher H contents is presumably a result of the relatively large homogeneity range of the hydride phase (see below). Upon further cycling (data not shown), the equilibrium pressure decreases well below 1 bar even at elevated temperatures. In fact, attempts to desorb the sample at room temperature by pumping it down to a pressure of $10^{-2}$ bar did not result in a noticeable hydrogen loss during a period of 24 h. Only desorption at 100 °C leads to a complete loss of hydrogen within 1.5 h. The second cycle of hydrogenation showed much faster kinetics while requiring a lower pressure: a weight increase of 0.76% corresponding to ∼2.5 H/f.u. was achieved within 30 min at 25 °C and 1 bar of hydrogen.

To estimate the maximum hydrogen content, we collected a set of consecutive XRD patterns for one of the deuteride samples immediately after opening the autoclave (100 bar, 2 days at room temperature). The observed volume expansion was +13.5% after 1 h, +13.2% after 7 h, +13.0% after 15 h, and +11.8% after two weeks of the sample standing in air. Extrapolating these values to the moment at which the autoclave was opened yielded a likely upper H content close to stoichiometric composition $LaNi_3BH_3$ (0.92 wt % hydrogen). The experimentally measured hydrogen capacity is in the range 0.7−0.84 wt %.

**Hydrogen-Induced Cell Expansion and Symmetry Change.** Hydrogenation of $LaNi_3B$ induces a symmetry change from *Imma* to *Bmmb* (nonstandard space group setting). At the transition, the structure expands in the *a*−*b* plane by ∼8% and contracts along the *c* axis (*b* in standard *Cmcm*) by ∼3%. In-situ X-ray measurements (data not shown) revealed that the contraction continues after the transition within the solid solution range $LaNi_3BH_x$ as *x* increases from 2.5 to 3. A contraction of that magnitude is unusual in metal−hydrogen systems. The largest cell contraction known, so far, is that in the basal plane of the hexagonal $RNiInD_{1.33}$ (R = La−Nd) with a ZrNiAl-type metal substructure (up to 4%) whose symmetry is preserved during hydrogenation.[31] For the $LaNi_3B-H_2$ system, the cell contraction correlates with the rearrangement of the lantha-

(28) Mattausch, H.; Simon, A.; Felser, C.; Dronskowski, R. *Angew. Chem., Int. Ed. Engl.* **1996**, *35*, 1685−1687.
(29) Brese, N. E.; O'Keeffe, M. *Acta Crystallogr. B* **1991**, *47*, 192−197.
(30) Niewa, R.; Zherebtsov, D. A.; Schnelle, W.; Wagner, F. R. *Inorg. Chem.* **2004**, *43*, 6188−6194.
(31) Vajeeston, P.; Ravindran, P.; Fjellvåg, H.; Kjekshus, A. *Phys. Rev. B* **2004**, *70*, 014107.

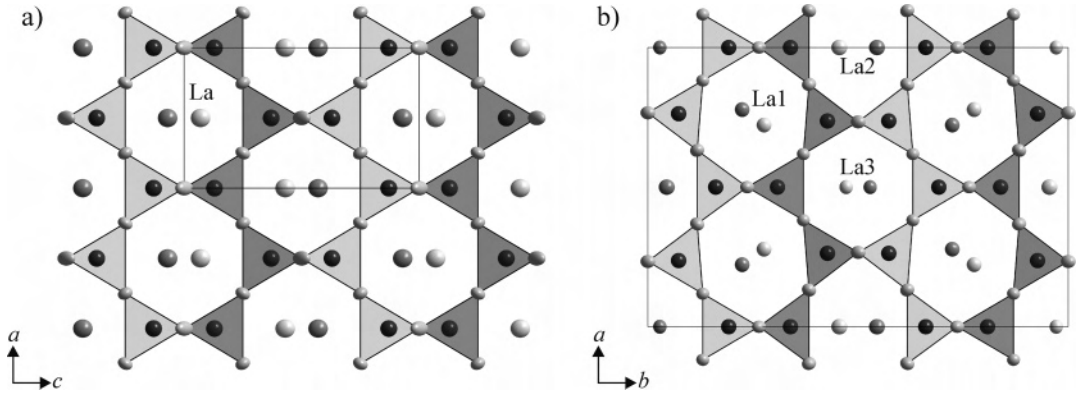


**Figure 6.** Tiling of the boron-centered Ni prisms (viewed along the prism axes) in (a) $LaNi_3B$ and (b) $LaNi_3BH_{\sim 2.7}$. Prisms and lanthanum atoms marked in light and dark are 1/2 apart along the eye's view. Rearrangement of the La atoms within the channels upon hydrogenation entails uniaxial cell contraction along the *c* axis (*b* in the hydride). Anisotropic thermal ellipsoids drawn at (a) 95% and (b) 50% probability levels (single-crystal XRD).

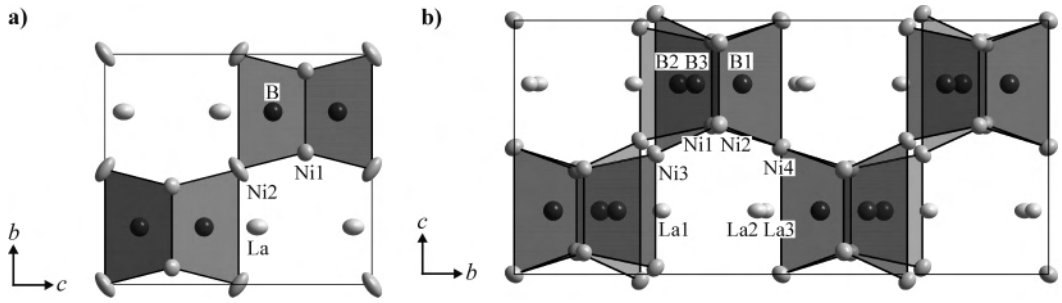


**Figure 7.** Structures of (a) $LaNi_3B$ and (b) $LaNi_3BH_{\sim 2.7}$ viewed along the *a axis* (i.e., perpendicular to the view direction in Figure 6). Thermal ellipsoids in the alloy structure predict the site symmetry lowering observed in the structure of the hydride.

num atoms in the channels of a nickel−boron framework (compare panels a and b of Figure 6).

The $LaNi_3B \rightarrow LaNi_3BH_x$ structure transition can be described by the group−subgroup chain *Imma* → [2] *Pmmb* → [2] *Bmmb* ($a' = 2a$, $c' = 2c$; for the standard setting, *Cmcm* $b'$ and $c'$ need to be interchanged). Although the intermediate space group *Pmmb* did not manifest itself experimentally, it is the only one possible according to the group−subgroup analysis. The symmetry reduction *Imma* → *Cmcm* leads to a quadruple cell and a splitting of Wyckoff positions (see Table 2): La and B sites are split into three sites each (4*e* → one 8*g* and two 4*c*), the two Ni sites are split into two sites each (8*g* → two 16*h*; 4*a* → one 8*f* and one 8*e*).

To our knowledge, this is the first example of a hydrogen-induced structure transition characterized on the same single crystal. Crystal fragmentation, twinning as a result of crack formation, is often inevitable when anisotropic or considerable isotropic cell expansion occurs. In the present study, the use of an image-plate detector in the diffraction experiment was essential because it allowed us to rapidly collect data on a crystal that desorbed hydrogen and at the same time detect crystal twinning and properly process it. High-resolution synchrotron powder diffraction on alloy and hydride samples confirmed the observed structure transition, resulting in a single-crystal-like quality for the structural parameters derived by Rietveld refinement.

**Structure of $LaNi_3BD_{\sim 2.7}$.** Apart from symmetry and cell expansion, the most striking change in the metal host structure concerns the arrangement of the boron and lanthanum atoms. The bicapped prismatic $[Ni_6La_2]$ boron atom coordination in the alloy (B−La = 2.98 Å) splits into monocapped $[Ni_6La]$ (B1), uncapped $[Ni_6]$ (B2), and bicapped prismatic $[Ni_6La_2]$ (B3) in the hydride (i.e., some La atoms (La1, La2) leave the coordination sphere during hydrogenation). Concomitantly, two nickel atoms of each La-capped $Ni_6$ prism have moved away from the B atoms at the center, thus increasing the B−Ni bond lengths (Table 3). These atoms (Ni3, Ni4) correspond to those in the alloy that show elongated thermal ellipsoids pointing into their shift direction during the hydrogenation-induced phase transition (see Ni2 in Figure 7a). Similar thermal displacement anisotropies correlating with the directions of the atomic shifts during composition-induced[32] or temperature-induced[33] structure transitions are known from other groups of compounds.

The deuterium atom arrangement is nearly ordered and consists of four almost fully occupied D sites with the following metal atom environments: deformed tetrahedral $La_2Ni_2$ (D1, D2), trigonal prismatic $La_3Ni_3$ (D3; short Ni−D, 1.70−1.89 Å, and long La−D, 2.70−2.88 Å, distances), and trigonal bipyramidal $La_2Ni_3$ (D4; base 2La + Ni, apexes 2Ni). The metal−deuterium distances are listed in Table 6. Lanthanum is connected by D1 and D2 into −La2−2D1−La1−2D2−La3− chains extending along the *a* axis and connected by D4 (La2−D4 = 2.39 Å) along the *c* axis. Each Ni atom has two boron ligands and either two (Ni1, Ni2) or

(32) Yashima, M.; Hirose, T.; Katano, S.; Suzuki, Y.; Kakihana, M.; Yoshimura, M. *Phys. Rev. B* **1995**, *51*, 8018−8025.
(33) Troyanov, S. I.; Kosterina, E. V.; Loose, A.; Reehuis, M.; Kemnitz, E. *Z. Kristallogr.* **2003**, *218*, 470−474.

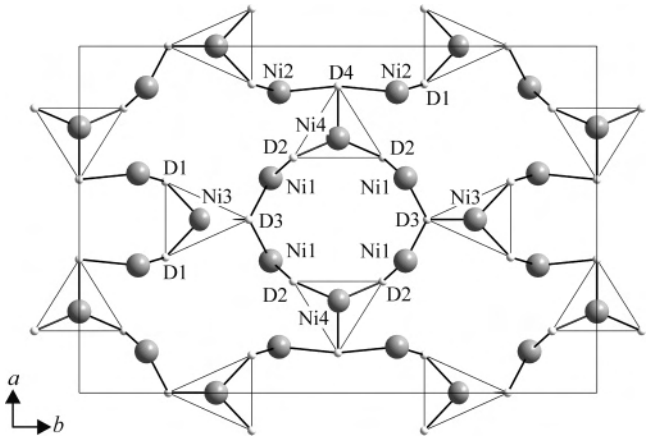


**Figure 8.** Two-dimensional framework of nickel−deuterium bonds in $LaNi_3BD_{\sim 2.7}$. The Ni3 and Ni4 atoms have trigonal-planar coordination by D atoms (Ni−D 1.62−1.70 Å, D−Ni−D 89−138°), while Ni1 and Ni2 have a 2-fold (Ni−D 1.62−1.97 Å, D−Ni−D 83−100°) D atom environment.

three (Ni3, Ni4) deuterium ligands that form the following configurations: a cis-square $B_2D_2$ for Ni1, a strongly distorted $B_2D_2$ tetrahedron for Ni2, an asymmetric trigonal bipyramid $B_2D_3$ (three basal D atoms at 1.67−1.70 Å and two apical B atoms at 2.02 and 2.46 Å) for Ni3, and a symmetric trigonal bipyramid $B_2D_3$ (three basal D atoms at 1.62−1.69 Å and two equidistant B atoms in apical positions at 2.20 Å) for Ni4.

**Ni−D Bonding and Boron-Induced D Atom Ordering.** From a bonding point of view, a more satisfactory description of the D atom distribution is in terms of a quasi two-dimensional puckered $[NiD]^-$ framework running parallel to the *a*−*b* plane (see Figure 8). Adjacent frameworks along the *c* axis are separated by planes of La and B atoms (Figure 7) and are connected via short Ni2−Ni2 contacts (2.44 Å). There is no D−Ni−D bridge between adjacent frameworks along *c*. Deuterium in the $[NiD]^-$ framework forms 3c−2e and 4c−2e bonds corresponding to the limiting ionic formula $La^{3+}B^0[Ni_3D_3]^{3-}$ for the fully deuterided state. From this formulation, one expects nickel to have a nearly closed-shell $3d^{10}$ electron configuration and hydrogen to act as an electron sink forming the previously free conduction electrons into localized metal−hydrogen bonds. This description is supported by bond-valence calculations;[29] they show that deuterium atoms are involved more in the D−Ni interactions than in the D−La interactions. This is particularly true for site D3; the D3−Ni distances are shorter than the D3−La distances (Table 6) by 1 Å thus suggesting a trigonal ($Ni_3$) metal environment rather than a trigonal prismatic ($La_3Ni_3$) metal environment. The D−Ni bond-valence sums are close to 1 for each of four deuterium atom sites, while the D−La bond-valence sums are considerably smaller (Table 7). The calculations also reveal the competition between deuterium and boron in the structure. As can be seen from Tables 6 and 7, lanthanum shows either relatively large La−D bond-valence sums and relatively long La−B distances for La2 or the inverse for La1 and La3, while nickel shows either relatively small Ni−D bond-valence sums and relatively short Ni−B distances for Ni1 and Ni2 or the inverse for Ni3 and Ni4. Thus, boron can be considered to be a competitor for deuterium in their interactions with lanthanum and nickel. Like $LaNi_4BH_x$,[5,7] the La−B planes in $LaNi_3BD_{\sim 2.7}$ do not accommodate deuterium. The B−D and D−D interactions appear to be repulsive: the shortest B−D and D−D contacts are 2.52 and 2.33 Å, respectively, and the B−B distances are greater than 3 Å. All of these observations suggest that the boron atoms, while being firmly fixed in the metallic structure, produce repulsive B−D interactions that tend to localize the hydrogen atoms in the structure and block hydrogen diffusion.[5,7] This is further supported by the fact that none of the interstitials, geometrically suitable for hydrogen occupation but possessing a boron atom in its environment, are actually filled by hydrogen. Attempts to predict hydrogen site occupancies on purely geometrical grounds, such as by Westlake's criteria (minimum hole size 0.4 Å, H−H distance >2.1 Å),[34] were unsuccessful. An illustrative example of this failure is provided by the $Ni_6$ prisms that are not occupied by boron. In the alloy structure, and according to the above criteria, these prisms and their surrounding lanthanum atoms form voids that are big enough to accommodate one hydrogen atom but not two hydrogen atoms as was observed experimentally. The presence of a second hydrogen atom in this void is, of course, a result of the relaxation of the metal atoms (La, Ni) during hydrogenation. Clearly, the direction and magnitude of these relaxations and the resulting superstructure of the hydride cannot be predicted from the alloy structure on purely geometrical grounds. They suggest the influence of other factors, such as boron-induced hydrogen ordering from repulsive boron−hydrogen interactions, and the tendency to form a covalently bonded nickel−hydrogen framework.

**Table 7.** Bond-Valence Sums for Deuterium Atoms in the $LaNi_3BD_{2.7}$ Structure (single-bond distances used: Ni−H 1.40 Å, La−H 2.06 Å)[29]

| | | | | | | | |
|---|---|---|---|---|---|---|---|
| D1−Ni | 1.04 | D1−La | 0.66 | La1−D | 1.59 | Ni1−D | 0.76 |
| D2−Ni | 0.95 | D2−La | 0.61 | La2−D | 2.58 | Ni2−D | 0.77 |
| D3−Ni | 0.98 | D3−La | 0.40 | La3−D | 1.75 | Ni3−D | 1.41 |
| D4−Ni | 0.99 | D4−La | 0.81 | | | Ni4−D | 1.47 |

**Acknowledgment.** This work was supported by the Swiss National Science Foundation and the Swiss Federal Office of Energy. It was partially performed at the Swiss Spallation Neutron Source SINQ at the Paul Scherrer Institute in Villigen, Switzerland, and at Swiss−Norwegian beamline SNBL at ESRF in Grenoble, France. Y.E.F. gratefully acknowledges Dr. Lukaš Palatinus (Institute of Physics, Prague, Czech Republic) for performing the MEM calculations and Dr. Alla Arakcheeva (EPFL, Lausanne, Switzerland) for fruitful discussions.

**Supporting Information Available:** Structural data as cif files, table with MEM results for the $LaNi_3B$ crystal, and a drawing of the residual electron density reconstructed with MEM. This material is available free of charge via the Internet at http://pubs.acs.org.

IC050416J

(34) Westlake, D. G. *J. Less-Common Met.* **1980**, *75*, 177−185.
(35) Bader, R. F. W. *Atoms in Molecules: A Quantum Theory*; Oxford University Press: Oxford, U.K., 1990.